Melting Behaviors, Isothermal Crystallization Kinetics, and Morphology of Poly(trimethylene terephthalate)/ Stainless Steel Fiber Composites

Chenguang Yao,[1,2] Tingxiu Xie,[3] Guisheng Yang[1,3]

[1]*Key Laboratory of Engineering Plastics, Joint Laboratory of Polymer Science and Technology, Institute of Chemistry, Chinese Academy of Sciences, Beijing 100080, People's Republic of China*
[2]*Graduate University, Chinese Academy of Sciences, Beijing 100039, People's Republic of China*
[3]*Shanghai Genius Advanced Material Company, Limited, Shanghai 201109, People's Republic of China*

Received 4 December 2007; accepted 24 March 2008
DOI 10.1002/app.28419
Published online 2 June 2008 in Wiley InterScience (www.interscience.wiley.com).

ABSTRACT: The melting behavior and crystallization kinetics of poly(trimethylene terephthalate) (PTT)/stainless steel fiber (SSF) composites were investigated with differential scanning calorimetry. The morphology was studied with scanning electron microscopy and polarized optical microscopy. Differential scanning calorimetry analysis revealed that the crystallization temperature increased by 27°C with the addition of 1 vol % SSF to the matrix. The Avrami exponents, analyzed in isothermal crystallization kinetics, were determined to be 2–3 for both neat PTT and PTT/SSF composites. SSF, as a nucleating agent in the composites, greatly increased the crystallization rate. The activation energies of the composites were obviously lower than that of pure PTT, and this indicated much easier crystallization of the composites. All these samples exhibited banded spherulites, and the spherulite size gradually decreased with the SSF loading increasing. Subsequent melting behaviors revealed that all of these samples, especially of the composites, exhibited triple melting peaks at all crystallization temperatures studied. © 2008 Wiley Periodicals, Inc. J Appl Polym Sci 109: 3562–3570, 2008

Key words: composites; crystal structures; crystallization; differential scanning calorimetry (DSC); spherulites

INTRODUCTION

Linear, aromatic, saturated polyesters such as poly (ethylene terephthalate) and poly(butylene terephthalate), because of their outstanding properties and inexpensive price, have been used as synthetic fibers, films, and engineering plastics for many years. However, poly(trimethylene terephthalate) (PTT) had not been commercialized until the breakthrough in the manufacturing cost of 1,3-propanediol. Recently, PTT has drawn much attention for its outstanding properties, such as good tensile behavior, resilience, outstanding elastic recovery, and dyeability. Moreover, it has an unusual combination of the topping properties of poly(ethylene terephthalate) and the processing characteristics of poly(butylene terephthalate). These characteristics make PTT suitable for applications in fibers, films, and engineering thermoplastics.[1,2]

There has been much research on the morphology,[3–7] crystallization kinetics,[4–15] rheological properties,[16–18] and mechanical properties[19–25] of PTT and its composites. Wu and Woo[3] investigated the ringed spherulite morphology of PTT with polarized optical microscopy (POM) and found that the rings in PTT may be related to multiple lamellae in the spherulites. Run et al.[6] studied the crystal morphology and nonisothermal crystallization kinetics of PTT/short-carbon fiber (SCF) composites, and they found that the diameter of the spherulites became smaller with an increasing content of SCF in the composites; also, the addition of SCF led to the formation of banded spherulites in the composites. Hu and Lesser[15] studied the nonisothermal crystallization of PTT/clay nanocomposites, and they found that the addition of clay to PTT increased the crystallinity and crystallization rate and that PTT/modified clay nanocomposites had a higher crystallization rate parameter than unmodified clay/PTT composites, so modified nanoscale clays are more effective nucleating agents than unmodified clay.

Plastics loaded with fibers such as carbon fibers, stainless steel fibers (SSFs), copper fibers, or metal-coated fibers have been widely used as electromagnetic shielding and engineering materials.[26] In this study, various PTT/SSF composites with different SSF contents were prepared with a corotating twin-screw extruder. The effects of the SSF loading on the

Correspondence to: G. Yang (ygs@geniuscn.com).
Contract grant sponsor: Shanghai Genius Advanced Material Co., Ltd.

© 2008 Wiley Periodicals, Inc.

crystallization kinetics and morphology of the composites were investigated with differential scanning calorimetry (DSC) and POM, respectively. To the best of our knowledge, few reports on the crystal morphology and isothermal crystallization kinetics of PTT/SSF composites can be found in the literature.

EXPERIMENTAL

Materials

The PTT homopolymer used in this study was supplied by Shell Chemicals (Houston, TX); it had an intrinsic viscosity of 0.94 dL/g in a phenol/tetrachloroethane (50/50 w/w) solution at 25°C. SSF was supplied by Koolon Fiber Technology Co. (Beijing, China); it was a high-quality alloy (18% chrome, 8–9% nickel, <2% manganese, and 80–95% martensite) and had an average length of 10 mm and a diameter of 8 μm, which led to a high length/diameter aspect ratio of 1250. Tetraisopropyl di(dioctylphosphate) titanate (KR-41B), which has good stability under 285°C, was supplied by Nanjing Lipai Chemical Co., Ltd. (Nanjing, China), and was used to modify SSF.

Fabrication of the PTT/SSF composites

SSF was dried at 110°C for 8 h and was added to a flask equipped with a reflux condenser. Ten parts by weight of tetraisopropyl di(dioctylphosphate) titanate, dissolved in 50 parts of ethanol with stirring, was added to the flask, and then the flask was heated to 100°C and kept for 20 min to obtain modified SSF. The modified SSF was dried at 60°C for 4 h to remove ethanol. PTT was dried in a vacuum oven at 140°C for 12 h to avoid moisture-induced degradation reactions. The master batch was first prepared by the melt compounding of dried PTT pellets and modified SSF at an SSF/PTT weight ratio of 1:4 in a twin-screw extruder at a die temperature of 251°C and a screw speed of 140 rpm; after being quenched in cold water, cut into pellets, and dried in a vacuum oven at 140°C for 12 h, the master batch was blended with neat PTT and allowed to reach a range of SSF contents of 2.9–19.6% w/w (0.5–4.0% v/v). With respect to the volume percentage of SSF, the composites were designated S0 (0% SSF), S1 (0.5% SSF), S2 (1% SSF), S3 (2% SSF), and S4 (4% SSF).

Analysis

The morphology of SSF in a PTT matrix was characterized with a JSM (Tokyo, Japan) 5600 LV scanning electron microscope. Samples for POM measurements were prepared through the sandwiching of a tiny pellet of a PTT/SSF composite between two glass plates, which was compressed at 260°C for 5 min in nitrogen and annealed in an oven at 200°C for 3 h. POM observations were performed with an Olympus BX51-P (Tokyo, Japan).

The melting and crystallization behaviors of five samples were investigated with the following program: the dried samples were first heated at a heating rate of 40°C/min from room temperature to 260°C under a nitrogen atmosphere, held for 5 min, cooled to 0°C at a cooling rate of 200°C/min to reach an amorphous state, then heated again at a rate of 10°C/min to 260°C, held for 5 min, and cooled to 50°C at a rate of 10°C/min. The second heating and cooling processes were recorded with a PerkinElmer (Shelton, CT) Diamond DSC instrument.

Isothermal crystallization and subsequent melting processes were performed as follows: the samples were heated at a rate of 40°C/min to 260°C, held for 5 min, cooled to the designated crystallization temperature (T_c) rapidly (200°C/min), held for certain time to ensure completion of the crystallization, and heated to 260°C again at a rate of 10°C/min after the isothermal crystallization was finished.

RESULTS AND DISCUSSION

Morphology

Scanning electron micrographs of composites brittle-fractured in liquid nitrogen are shown in Figure 1. SSF is dispersed uniformly in the matrix, and there is no obvious agglomeration, as also confirmed by Figure 2(d,e). These results suggest that the shear force of melt extrusion is strong enough to break down all the agglomerations, even at a high SSF loading (e.g., 4 vol %).

Figure 2(a–e) shows a series of POM micrographs for PTT and composites isothermally crystallized at 200°C for 3 h. Figure 2(a,b) reveals the well-defined and large spherulitic morphology of pure PTT. The largest spherulites can reach a diameter of 1 mm [e.g., Fig. 2(b)]. Spherulites impinge on one another and form particular polygonal spherulites with clear boundaries. However, Figure 2(c–e) shows a poor spherulitic morphology with respect to pure PTT; in other words, with increasing SSF loading, the spherulite size gradually decreases with less perfection as interspherulitic interactions increase. These results indicate that SSF or its particles produced during processing can act as seeds for spherulite growth. As the spherulites grow, they are confined by one another and SSF as well, and this leads to more spherulites forming in a limited space. Furthermore, the optical behavior of these spherulites exhibits typical mixed birefringence (i.e., the first and third quadrants of the spherulites and the second and fourth quadrants all exhibit the same color). Furthermore, all of the spherulites are banded spherulites.

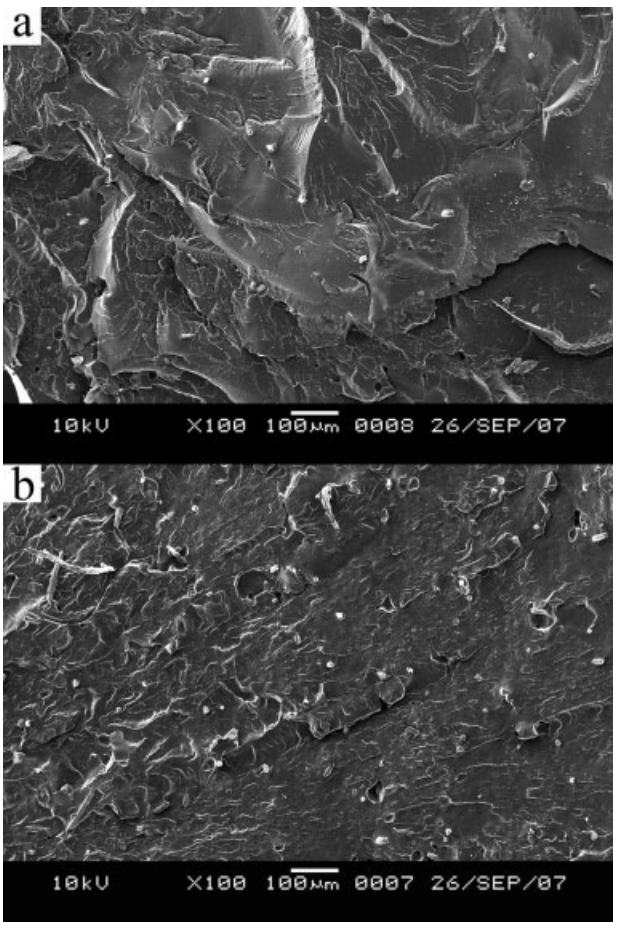

Figure 1 Scanning electron micrographs of composites with different SSF contents: (a) S1 and (b) S3.

The banded spherulite phenomenon of PTT has been previously studied.[4] The appearance of banded spherulites in PTT is strongly dependent on the level of T_c; at lower T_c's (<195°C), the banded morphology disappears, and a regular spherulite image is exhibited; a temperature higher than 195°C will induce the formation of banded spherulites. In our study, T_c of the samples was 200°C, so banded spherulites were observed as expected.

Melting and crystallization behaviors

Typical melting DSC curves of the five samples are shown in Figure 3. The kinetic parameters of the melting process are summarized in Table I. Neat PTT exhibits an apparent glass transition at about 50.5°C, a cold-crystallization peak at about 77.3°C, and a melting peak at about 230°C. However, neither an obvious glass transition nor cold crystallization is observed for S1–S4. The appearance of a cold-crystallization peak in neat PTT suggests that at the cooling rate of 200°C/min, molten PTT is frozen to the amorphous state directly, whereas the molten composites (S1–S4) are essentially turned into semicrystalline ones at the same cooling rate. Moreover, an obvious recrystallization peak can be observed around 210°C in each curve of the composites, whereas no recrystallization peak is shown in the curve of neat PTT; this indicates that semicrystalline S1–S4 are more likely to undergo a melting/recrystallization process during DSC scanning.[7] Comparing the melting enthalpy (ΔH_m) and crystallization enthalpy (ΔH_c) of the composites with those of pure PTT, we find that the composites exhibit higher values, and this implies that the addition of SSF enhances the degree of crystallinity of PTT.

The melt-crystallization behaviors of five composites at the cooling rate of 10°C/min are shown in Figure 4. The kinetic parameters of the cooling process are also summarized in Table I. As shown in Figure 4, the crystallization exothermal peaks of S1–S4 shift to high temperatures in comparison with neat PTT, and this suggests that SSF or its particles produced during processing greatly increase the melt-crystallization temperature. In detail, with an increasing loading of SSF, the melt-crystallization temperature of the composites increases to a maximum at 1 vol % SSF and changes little subsequently. Actually, there are two factors controlling the crystallization of polymeric composite systems. One is that additives have a nucleating effect, which results in an increase in T_c, a positive effect on crystallization. The other is that the additives hinder the migration and diffusion of polymer molecular chains to the surface of the nucleus, and they constrain spherulitic growth by an impingement mechanism in the composites, which results in decreasing T_c, a negative effect on crystallization. In this case, the negative effect gradually increases with increasing SSF content and comes to a head at 1 vol % SSF, at which the melt-crystallization temperature is maximum.

Isothermal crystallization kinetic analysis

Isothermal crystallization behaviors

An exothermal diagram of the isothermal crystallization analysis for S2 is shown in Figure 5 (others are omitted because they have similar shapes). With T_c increasing, the exothermal peak of each curve shifts to longer times, and this indicates that T_c is an important influencing factor for determining the crystallization time. As shown in Table II, ΔH_c of each sample increases slightly with increasing T_c. By comparing ΔH_c of the composites at the same T_c value, we find that ΔH_c gradually increases with increasing SSF loading, and this indicates that SSF enhances the total crystallization of the composites.

Figure 6 presents the relative crystallinity at time t [$X_c(t)$] integrated from Figure 5 as a function of crys-

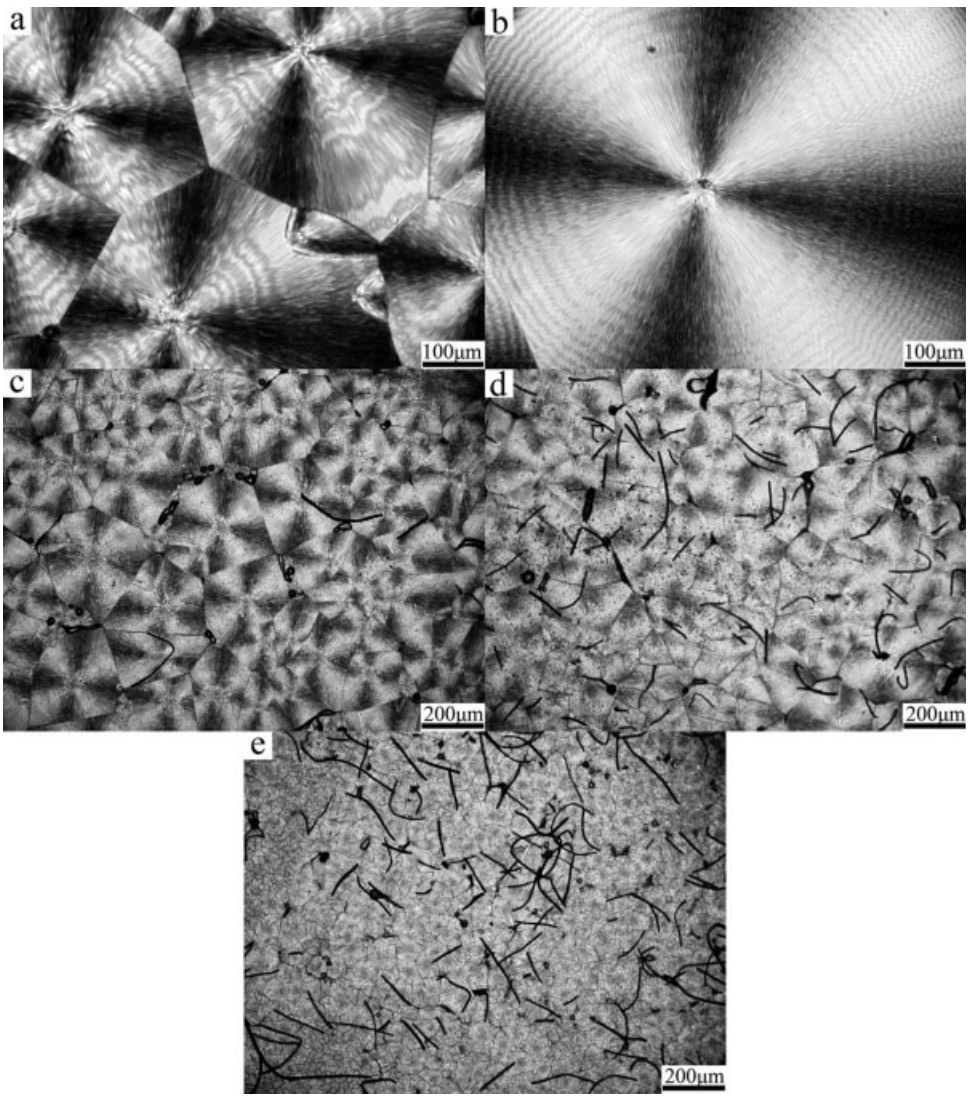

Figure 2 Polarized microscopy pictures of the crystallized composites: (a,b) S0, (c) S1, (d) S2, and (e) S3.

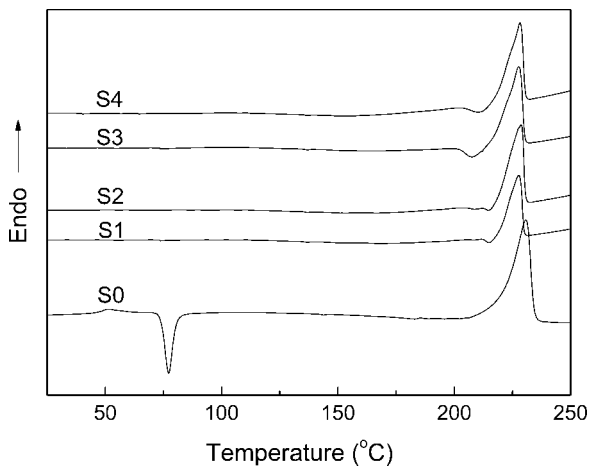

Figure 3 Second-heating DSC curves of the PTT/SSF composites.

tallization time t for S2 at various T_c values (others are omitted because they have similar shapes). In Figure 6, the characteristic sigmoidal isotherms are shifted to the right along the time axis with increasing T_c, and this suggests a progressively slower crystallization rate as T_c increases.

Another important parameter is the half-time of crystallization ($t_{1/2}$), which is defined as the time taken from the onset of $X_c(t)$ until 50% completion. $t_{1/2}$ of various samples is listed in Table II. $t_{1/2}$ of neat PTT increases sharply as T_c increases from 188 to 194°C, and this indicates that neat PTT is a thermally activated crystallization polymer. The composites show slow changes in $t_{1/2}$ in comparison with pure PTT with increasing T_c, and this indicates less dependence on T_c for the composites than for the neat polymer. When T_c is 190°C (Table II), $t_{1/2}$ of

TABLE I
Kinetic Parameters of Melting and Crystallization for Various Samples

	Heating scan					Cooling scan	
Sample	T_g (°C)[a]	$T_{c,c}$ (°C)[b]	T_{rec} (°C)	T_m (°C)[c]	ΔH_m (J/g)	$T_{m,c}$ (°C)[d]	ΔH_c (J/g)
S0	50.5	77.3	—	230.0	43.2	162.6	−48.2
S1	—	—	215.0	227.5	47.0	178.8	−51.0
S2	—	—	214.8	228.5	49.4	189.6	−51.7
S3	—	—	207.9	227.5	52.1	188.9	−52.3
S4	—	—	211.1	228.0	54.2	188.0	−53.2

[a] Glass-transition temperature.
[b] Temperature of the cold-crystallization peak in the heating scan.
[c] Melting temperature.
[d] Temperature of the melt-crystallization peak in the cooling scan.

neat PTT is evidently longer than that of the composites, and this suggests an apparent increase in the crystallization rate when SSF is loaded into the polymer matrix. From the results, we also find that S2 has the lowest $t_{1/2}$ value of the five samples; that is, S2 has the fastest crystallization rate (for the reasons, see the last paragraph of the next section).

Analysis based on the Avrami equation

If we assume that $X_c(t)$ increases with crystallization time t, the Avrami equation can be used to analyze the isothermal crystallization process of neat PTT and PTT/SSF composites as follows:[28,29]

$$1 - X_c(t) = \exp(-Z_t t^n) \quad (1)$$

$$\log[-\ln(1 - X_c(t))] = n \log t + \log Z_t \quad (2)$$

where Avrami exponent n is a mechanism constant with a value depending on the type of nucleation and the growth dimension and Z_t is a growth rate constant involving both nucleation and growth rate parameters. Plots of $\log\{-\ln[1 - X_c(t)]\}$ versus $\log t$ according to eq. (2) for S2 are shown in Figure 7 (others are omitted because they have similar shapes). The experimental data appear to fit very well with the Avrami equation at the primary crystallization stage.

n and Z_t can readily be extracted from the Avrami plots in Figure 7, and their values for various samples are listed in Table II. In this work, the values of n increase from 2.5 to 2.7 for pure PTT in this temperature range according to the definition of n,[30] which corresponds to two-dimensional growth with a combination of thermal and athermal nucleation mechanisms (to pacify the fractional values of n observed). Without any heterogeneous nucleating agent, the crystal nucleus forms slowly and the molecular chains arrange very slowly at these T_c values. As a result, crystals with a lamellar form are the predominant components of the polymer. Actually, the temperature dependence of n should be that n increases with increasing T_c within the nucleation control region. This is because the number of athermal nuclei increases tremendously with decreasing T_c[31,32] and causes the nucleation mechanism to be

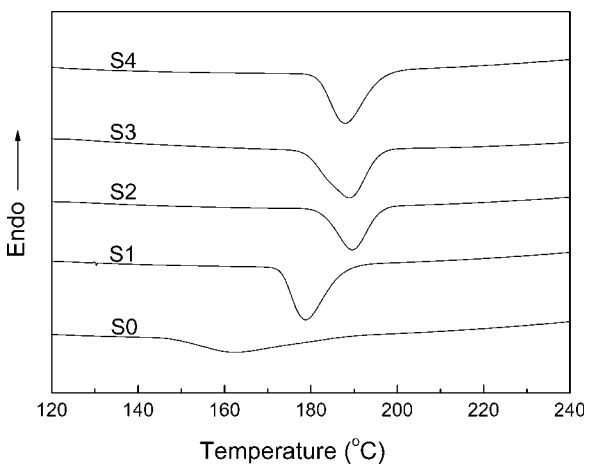

Figure 4 Melt-crystallization DSC curves of the PTT/SSF composites.

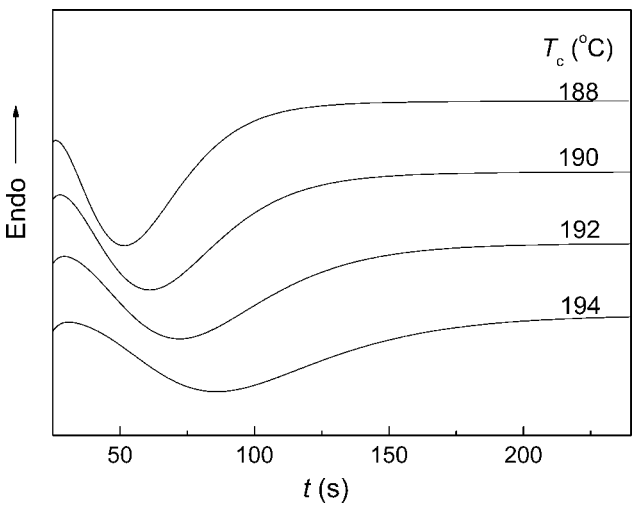

Figure 5 Heat flow versus time t during the isothermal crystallization of S2 at different T_c values by DSC.

TABLE II
Kinetic Parameters of Isothermal Crystallization for Various Samples

Sample	T_c (°C)	n	$Z_t \times 10^{-7}$ (s^{-n})	$t_{1/2}$ (s)	ΔH_c (J/g)
S0	188	2.5	83.2	278.4	−31.6
	190	2.5	52.5	345.2	−33.8
	192	2.6	6.8	434.7	−37.0
	194	2.7	1.8	561.5	−37.5
S1	188	2.5	1445.4	30.9	−31.8
	190	2.5	758.6	39.9	−35.9
	192	2.6	537.0	50.2	−39.2
	194	2.6	120.2	66.6	−41.7
S2	188	2.5	1949.8	25.3	−32.3
	190	2.5	1148.2	35.0	−35.1
	192	2.6	676.1	46.0	−39.3
	194	2.7	141.3	61.7	−42.5
S3	188	2.6	446.7	51.6	−39.8
	190	2.6	288.4	64.8	−40.6
	192	2.7	190.6	81.1	−42.6
	194	2.7	60.3	103.9	−43.9
S4	188	2.6	277.7	80.4	−39.8
	190	2.6	179.7	100.8	−40.0
	192	2.6	24.8	129.6	−41.6
	194	2.7	8.1	166.0	−41.8

more instantaneous in time and reduces the values of n.

These values of n for S1–S4 are all about 2.6 ± 0.1 and increase somewhat with increasing T_c; these may be average values of various nucleation types and growth dimensions occurring simultaneously in the crystallization process. For S1–S4 with SSF as a heterogeneous nucleus, the nucleation type should mostly be heterogeneous nucleation, and the growth dimension should mostly be a three-dimensional space extension. As a result, crystals with a spherical form are the predominant components in PTT composites.

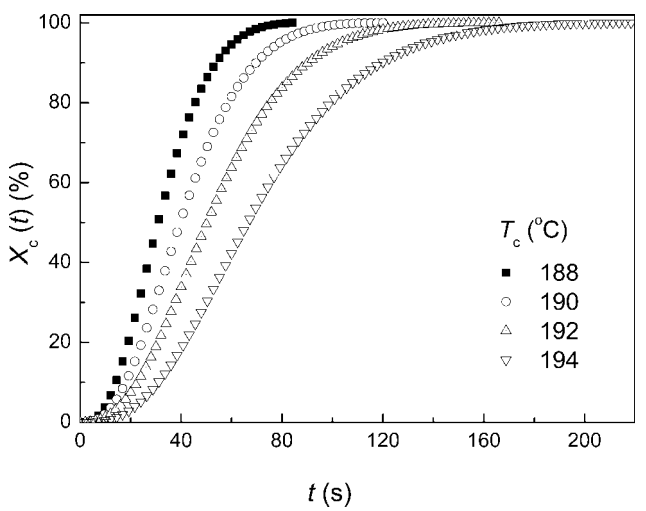

Figure 6 Development of $X_c(t)$ with time t for the isothermal crystallization of S2 at different T_c values.

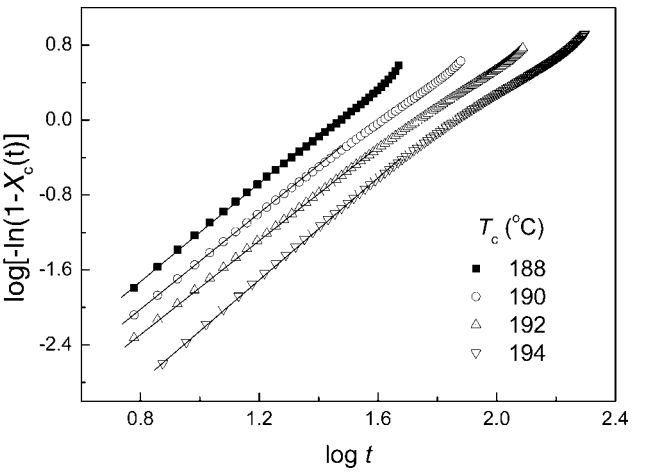

Figure 7 Plots of $\log\{-\ln[1 - X_c(t)]\}$ versus $\log t$ for S2 at the indicated temperatures.

As shown in Table II, another overall rate parameter (Z_t) determines both the nucleating and growth processes, which are extremely sensitive to temperature for each sample; that is, the higher the temperature is, the lower the crystallization rate is. Comparing the Z_t values of S0–S4 at the same T_c (e.g., 190°C), we find that Z_t of S1 and S2 increases sharply with respect to that of neat PTT, but Z_t of S3 and S4 is much lower than that of S1 and S2. These facts indicate that with the proper content of SSF in the composite, the crystallization rate will be greatly increased. However, too much SSF will reduce the crystallization rate. This is because fibers have a dual effect in the matrix[27] (as mentioned in the second paragraph of the Melting and Crystallization Behaviors section): on the one hand, fibers can enhance the crystallization rate by providing added surface nucleation sites; on the other hand, fibers can also depress the crystallization rate with respect to an unreinforced polymer because they hinder the migration and diffusion of polymer molecular chains to the surface of the nucleus and constrain spherulitic growth by an impingement mechanism. In this case, the effect of SSF on T_c of PTT is the result of the competition of these two factors. The constraining effect of fibers is relatively feeble at low SSF fractions (e.g., S1 and S2), and the enhancing effect plays a predominant role, whereas with the fiber loading increasing (e.g., S3 and S4), the constraining effect increases and the enhancing effect decreases, so the crystallization rate decreases accordingly.

Subsequent melting behaviors

The triple melting phenomenon of PTT has previously been reported;[3,11,12,14,16] Srimoaon et al.[12] investigated multiple melting behaviors in isothermally crystallized PTT using DSC, and they

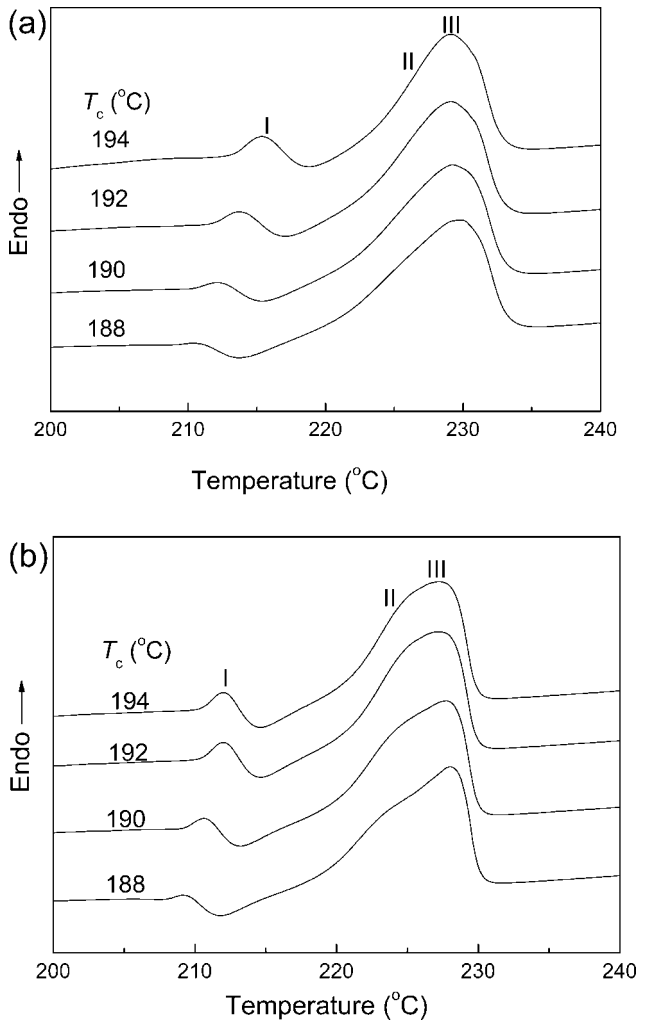

Figure 8 Melting endotherms of (a) S0 and (b) S2 composites recorded at a heating rate of 10°C/min after isothermal crystallization at the specified temperatures.

observed that the subsequent melting thermograms for PTT isothermally crystallized within the T_c range of 182–215°C exhibited a triple (for T_c values lower than ca. 192°C), double (for T_c values greater than ca. 192°C but lower than ca. 210°C), or single (for T_c values greater than ca. 210°C) endothermic melting phenomenon. For the triple melting phenomenon, Chung et al.[11] concluded that the occurrence of peak I at a lower temperature could be attributed to recrystallization during the reheating process, and peaks II and III at higher temperatures could be attributed to the melting of the primary crystallites of two populations of lamellar stacks.

Figure 8(a,b) shows DSC heating thermograms of neat PTT and PTT/SSF composites annealed at different T_c values, and the parameters are summarized in Table III. As shown in Figure 8(a,b) and Table III, it is apparent that the melting endotherms of neat PTT and especially the composites exhibit triple melting peaks at all T_c values studied; peaks I and II shift to higher temperatures as T_c increases from 188 to 194°C, whereas peak III changes little, and peaks II and III tend to combine. As shown in Figure 8(a,b), the area of peak III is larger than that of either peak I or II, and this indicates that the major crystallization of PTT is predominantly composed of primary crystals. Comparing the melting endotherms of neat PTT with those of S1–S4 at the same T_c (e.g., 188°C), we find that peaks I, II, and III of the composites are all lower than those of pure PTT; therefore, it can be concluded that SSF can induce the formation of crystallites with a smaller or poor morphology.

From Figure 8(a,b) and Table III, we can see that a recrystallization exotherm can be obtained during DSC heating, which tends to shift to a higher temperature as T_c increases. By comparing the recrystallization peak locations [i.e., the temperature of the recrystallization peak in the heating scan (T_{rec})] of the five samples at the same T_c (e.g., 190°C), we find that the T_{rec} values of the composites are all lower than that of neat PTT, and this indicates that the crystallites of the composites are smaller or less prefect and more likely to undergo a melting/recrystallization process during a heating scan. The melting enthalpy of peaks II and III ($\Delta H_{fII+III}$) increases somewhat for all the samples with increasing T_c; moreover, the value of $\Delta H_{fII+III}$ gradually increases with the SSF loading increasing at the same T_c (e.g., 190°C). This indicates that the addition of SSF enhances the degree of crystallinity of the composites.

Crystallization activation energy (ΔE)

The crystallization process of S0–S4 is assumed to be thermally activated. The crystallization rate parameter Z_t can be described by the following Arrhenius equation:[33]

$$Z_t^{1/n} = Z_0 \exp\left(\frac{-\Delta E}{RT_c}\right) \tag{3}$$

$$\left(\frac{1}{n}\right) \ln Z_t = \ln Z_0 - \frac{\Delta E}{RT_c} \tag{4}$$

where, Z_0 is a temperature-independent pre-exponential factor and R is the gas constant. ΔE can be determined by the slope coefficient of plots of $(1/n)\ln Z_t$ versus $1/T_c$, as shown in Figure 9. Because it has to release energy when the molten fluid is transformed into the crystalline state, the value of ΔE is negative according to the concept of heat quantity in physical chemistry. The ΔE values for five samples in the primary crystallization stage are −256.9 (S0), −168.8 (S1), −151.3 (S2), −195.4 (S3), and −200.2 kJ/mol (S4). ΔE of these composites decreases as the

TABLE III
Melting Endotherm Parameters of Various Samples

Sample	T_c (°C)	T_{mI} (°C)[a]	T_{mII} (°C)[b]	T_{mIII} (°C)[c]	$\Delta H_{fII+III}$ (J/g)	T_{rec} (°C)
S0	188	211.3	225.9	229.6	34.9	213.7
	190	212.2	226.3	229.3	36.4	215.5
	192	213.8	226.1	229.2	36.9	217.0
	194	215.4	226.5	229.2	37.5	218.7
S1	188	209.6	223.2	228.0	37.0	211.8
	190	210.7	224.2	227.7	37.0	213.2
	192	211.9	224.5	227.3	38.8	214.6
	194	212.0	224.9	227.4	38.8	214.6
S2	188	209.7	223.6	228.3	43.3	212.2
	190	210.9	224.0	228.0	44.0	213.5
	192	212.2	224.8	227.8	45.0	215.1
	194	213.6	225.4	227.8	45.3	216.5
S3	188	209.7	223.9	227.7	48.2	212.2
	190	210.9	224.0	228.0	48.8	213.8
	192	212.3	224.5	228.2	49.8	215.2
	194	213.8	225.0	227.8	50.5	216.8
S4	188	209.6	223.8	228.1	48.5	212.4
	190	211.1	224.3	227.6	48.6	214.0
	192	212.6	224.5	227.6	49.9	215.4
	194	213.9	225.2	227.6	51.0	216.9

[a] Melting temperature of peak I.
[b] Melting temperature of peak II.
[c] Melting temperature of peak III.

SSF loading increases to 1%, and this indicates that the proper content of SSF provides added surface nucleation sites or acts as a nucleating agent in the polymer matrix; this improves the nucleation rate and induces the arrangement of molecular chains on the surface of SSF. However, too many fibers (e.g., 4%) will increase ΔE and constrain the arrangement of molecular chains. It is interesting to note that S2 exhibits the lowest value of ΔE, which indicates that the nucleating effect (positive effect) and the constraining effect (negative effect) reach an equilibrium at 1 vol % SSF (see also the discussion in the second paragraph of the Melting and Crystallization Behaviors section and the fourth paragraph of the Analysis Based on the Avrami Equation section). This result is also confirmed by the conclusion of a relationship between Z_t, $t_{1/2}$, and the SSF content in the polymer matrix, as mentioned previously.

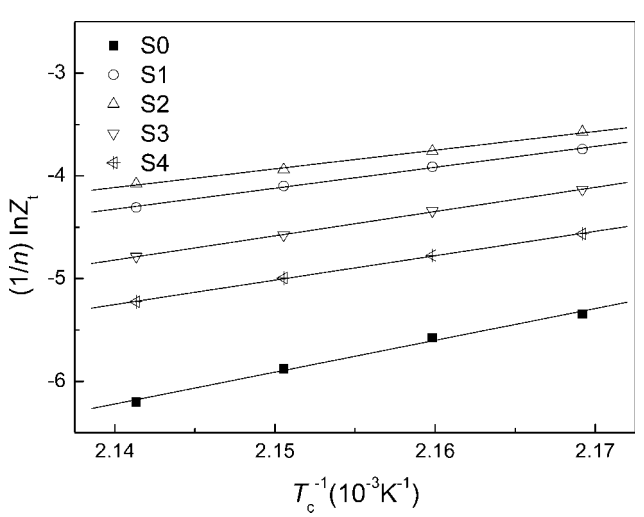

Figure 9 Plot of $(1/n)\ln Z_t$ versus $1/T_c$ for Avrami parameter Z_t deduced from the isothermal crystallization process.

An increase in the crystallization rate and a reduction of ΔE are common characteristics for polymer/inorganic particle composites.[15] Crystallization includes two processes: nucleation and growth. In this case, the addition of SSF has a positive effect on the nucleation process and a negative effect on the growth process, but the net influence is positive. Furthermore, in addition to the function of tetraisopropyl di(dioctylphosphate) titanate in lowering the surface free energy of SSF, part of the modifier also acts as a plasticizer for PTT, increasing the free volume of PTT. Therefore, the activation energy for the transport of PTT molecular segments to the crystallization front is reduced, and this leads to an increasing spherulite growth rate.

CONCLUSIONS

PTT/SSF composites have been evaluated with DSC, scanning electron microscopy, and POM. SSF in the PTT matrix is well dispersed, even though the volume content is up to 4%, as confirmed by scanning electron microscopy and POM. The addition of SSF greatly increases T_c of PTT. The maximal improvement is 27°C by the addition of 1 vol % SSF to the

matrix. At the primary stage of the isothermal crystallization process, the values of n have been determined to be 2–3 both for neat PTT and PTT/SSF composites. The results for $t_{1/2}$ and Z_t suggest that SSF, acting as a nucleation agent, can arouse and accelerate the crystallization of the composites and decrease the dimensions of the crystals. The subsequent melting behaviors of all the samples included triple melting peaks. Moreover, the activation energies of crystallization, calculated with the Arrhenius equation, show that the composites have higher crystallization ability than neat PTT. POM observations confirm that composites form much smaller, more uniform spherulites than neat PTT, and all the samples exhibited banded spherulites.

The authors thank Wenya Liu for the helpful guidance provided during the preparation of this article in English.

References

1. Wu, J.; Schultz, J. M.; Samon, J. M.; Pangelinan, A. B.; Chuah, H. H. Polymer 2001, 42, 7141.
2. Grande, J. A. Mod Plast 1997, 12, 97.
3. Wu, P. L.; Woo, E. M. J Polym Sci Part B: Polym Phys 2003, 41, 80.
4. Ho, R. M.; Ke, K. Z.; Chen, M. Macromolecules 2000, 33, 7529.
5. Wang, B. J.; Li, C. H.; Hanzlicek, J.; Cheng, S. Z. D.; Geil, P. H.; Grebowicz, J.; Ho, R. M. Polymer 2001, 42, 7171.
6. Run, M. T.; Song, H. Z.; Yao, C. G.; Gao, J. G. J Appl Polym Sci 2007, 106, 868.
7. Run, M. T.; Yao, C. G.; Wang, Y. J.; Gao, J. G. J Appl Polym Sci 2007, 106, 1557.
8. Xue, M. L.; Sheng, J.; Yu, Y. L.; Chuah, H. H. Eur Polym J 2004, 40, 811.
9. Huang, J. M.; Chang, F. C. J Polym Sci Part B: Polym Phys 2000, 38, 934.
10. Pyda, M.; Wunderlich, B. J Polym Sci Part B: Polym Phys 2000, 38, 622.
11. Chung, W. T.; Yeh, W. J.; Hong, P. D. J Appl Polym Sci 2002, 83, 2426.
12. Srimoaon, P.; Dangseeyun, N.; Supaphol, P. Eur Polym J 2004, 40, 599.
13. Hong, P. D.; Chung, W. T.; Hsu, C. F. Polymer 2002, 43, 3335.
14. Dangseeyun, N.; Srimoaon, P.; Supaphol, P.; Nithitanakul, M. Thermochim Acta 2004, 409, 63.
15. Hu, X. B.; Lesser, A. J. Macromol Chem Phys 2004, 205, 574.
16. Apiwanthanakorn, N.; Supaphol, P.; Nithitanakul, M. Polym Test 2004, 23, 817.
17. Supaphol, P.; Dangseeyun, N.; Thanomkiat, P.; Nithitanakul, M. J Polym Sci Part B: Polym Phys 2004, 42, 676.
18. Chen, K. Q.; Shen, J.; Tang, X. Z. J Appl Polym Sci 2005, 97, 705.
19. Shu, Y. C.; Hsiao, K. J. J Appl Polym Sci 2007, 103, 2387.
20. Hsiao, K. J.; Lee, S. P.; Kong, D. C.; Chen, F. L. J Appl Polym Sci 2006, 102, 1008.
21. Zhang, J. L.; Wu, L.; Zhao, M. L.; Li, J. C.; Wang, C. L. J Appl Polym Sci 2005, 96, 883.
22. Zhang, J. L. J Appl Polym Sci 2004, 91, 1657.
23. Ramiro, J.; Eguiazábal, J. I.; Nazábal, J. Polym Adv Technol 2003, 14, 129.
24. Chang, J. H.; Mu, K. M.; Kim, J. C. J Appl Polym Sci 2006, 102, 4535.
25. Mackintosh, A. R.; Liggat, J. J. J Appl Polym Sci 2004, 92, 2791.
26. Chen, S. C.; Chien, R. D.; Lee, P. H.; Huang, J. S. J Appl Polym Sci 2005, 98, 1072.
27. Liu, W. J.; Mohanty, A. K.; Drzal, L. T.; Misra, M.; Kurian, J. V.; Miller, R. W.; Strickland, N. Ind Eng Chem Res 2005, 44, 857.
28. Avrami, M. J Chem Phys 1940, 8, 212.
29. Avrami, M. J Chem Phys 1939, 7, 1103.
30. Wunderlich, B. Macromolecular Physics; Academic: New York, 1976; Vol. 2, p 132.
31. Supaphol, P.; Spruiell, J. E. J Appl Polym Sci 2000, 75, 337.
32. Janeschitz-Kriegl, H.; Ratajski, E.; Wippel, H. Colloid Polym Sci 1999, 277, 217.
33. Cebe, P.; Hong, S. D. Polymer 1986, 27, 1183.